Critical Size of Silver Iodide Containing Glaciogenic Cloud Seeding Particles

Jie Chen[1,][*], Carolin Rösch[1,#], Michael Rösch[1], Aleksei Shilin[2], Zamin A. Kanji[1,*]

[1]Institute for Atmospheric and Climate Science, ETH Zürich, Zurich, 8092, Switzerland

[#]Now at City of Zurich, Environment and Health Safety, Air Quality Division, Zurich Switzerland

[2]Cloud Seeding Technologies, Burgenstrasse 22, Gaertringen, 71116, Germany

[*] Corresponding authors:
Zamin A. Kanji zamin.kanji@env.ethz.ch and Jie Chen jie.chen@env.ethz.ch

Contents of this file

Introduction

The Supporting Information shows additional Figures (S1~S8) and Tables (S1~S2) providing detailed information on the experimental setup (Fig. S1~S3), validation of the ice nucleation chamber (Fig. S4), and size distribution and other analysis (Fig. S6-S8 and Table S1-S2) of cloud seeding aerosols generated in the present study.
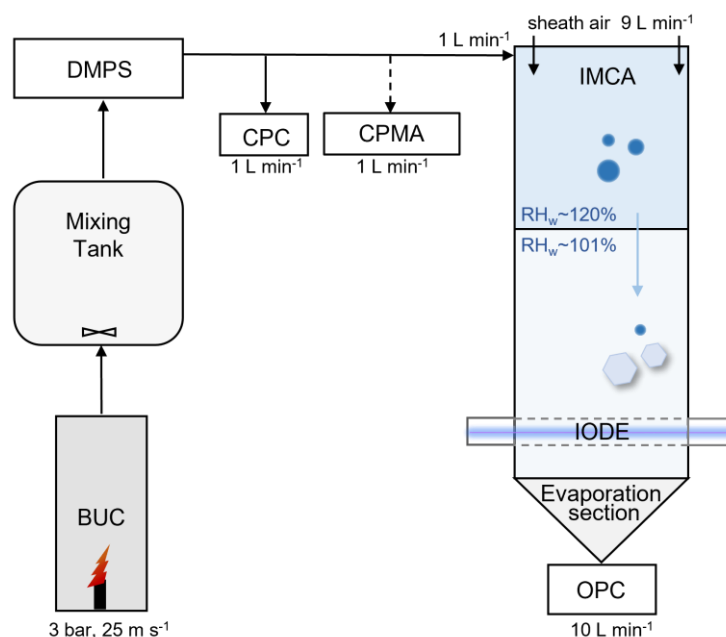
Figure S1. Schematic of the experimental setup for aerosol generation and dispersal, size selection, mass measurement and ice nucleation measurement in immersion freezing mode. BUC-burning chamber; DMPS-differential mobility particle spectrometer; CPMA-centrifugal particle mass analyzer; IMCA-immersion mode cooling chamber; CPC-condensation particle counter; ZINC-Zürich ice nucleation chamber; IODE-Ice Optical DEpolarization detector; OPC-optical particle counter.
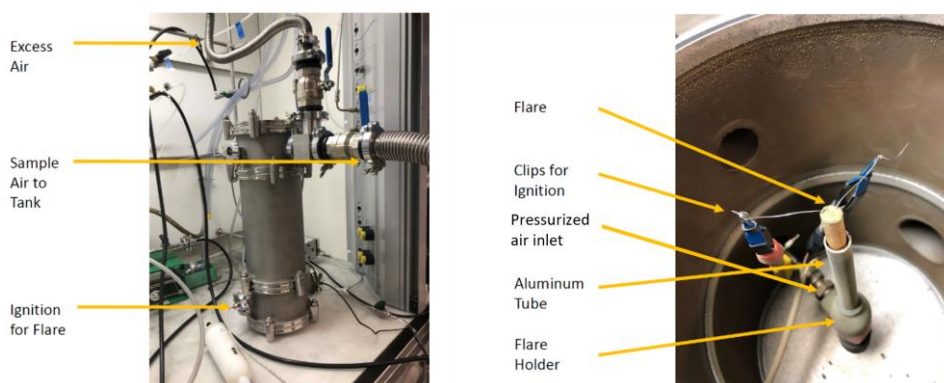

Figure S2. Left: Setup of the burning chamber (BUC) and right: a peek inside BUC.

Text S1. **Design of the burning chamber.** The BUC is made of stainless steel with a compressed air inlet and an excess air outlet at the top and bottom (Fig. S2, left). The flare is placed onto a customized 3D-printed holder, which is connected to the inlet for pressurized air (Fig. S2, right). The aluminum tube (diameter: 8 mm) surrounding the flare (diameter: 7 mm) is designed to increase the air velocity around the flame.

Text S2. **Working principle of differential mobility particle spectrometer (DMPS).** The DMPS includes a polonium source (neutralizer) and a differential mobility analyzer (Long DMA, model 3081; TSI Inc.). Electrostatically charged aerosol particles were passed through the polonium neutralizer which imparted a predictable charge distribution to

the particles. Within the DMA, defined charged particles are selected according to their electrical mobility, which is size-dependent. In a regular experiment, the aerosol and sheath flow rates in DMA were 2 L min^{-1} (or 3 L min^{-1} if the particle mass was measured by CPMA) and 8 L min^{-1} respectively (Fig. S1).

Text S3. **Working principle of centrifugal particle mass analyzer (CPMA).** CPMA is a commercial instrument to measure the particle mass of single particles. CPMA consists of two concentric metal cylinders, which are free to rotate separately. Particles are charged by the neutralizer (polonium source) before entering CPMA. The electrical and centrifugal fields within CPMA can be adjusted by changing the voltage between- and rotation speed of- the two cylinders. Only particles whose centrifugal and electrostatic forces balance (i.e., those with the correct mass: charge ratio as set by the combination of rotation and voltage) will pass through the CPMA.
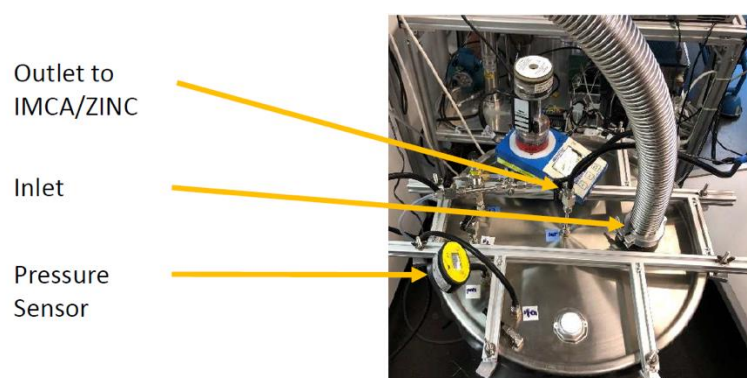

Figure S3. Setup of the small mixing tank. As indicated by the yellow arrows, the tank includes the inlet of nitrogen and the outlet to the IMCA-ZINC system. The pressure sensor is attached to avoid overpressure.

Text S4. **Validation of IMCA-ZINC.** The performance of the IMCA-ZINC system was tested and validated by measuring the homogeneous freezing of 200 nm diameter ammonium nitrate particles at temperatures down to 231 K (Fig. S4). The same approach was used by Lüönd et al. [2010] and Welti et al. [2012]. The good agreement between the phase transition of ammonium nitrate droplets obtained in the present study and those predicted by models [Earle et al., 2010; Ickes et al., 2015] validates the temperature performance of IMAC–ZINC in measuring the freezing ability of cloud droplets.
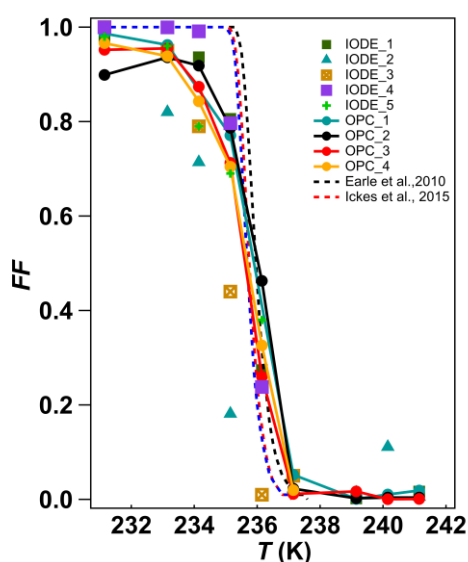

3

Figure S4. The frozen fraction (FF) of ammonium nitrate droplets as a function of temperature measured by the optical particle counter (OPC) and Ice Optical Detector (IODE) in repeated experiments; The dashed lines indicate the theoretically predicted freezing curves for pure water from *Earle et al.* [2010] and *Ickes et al.* [2015].
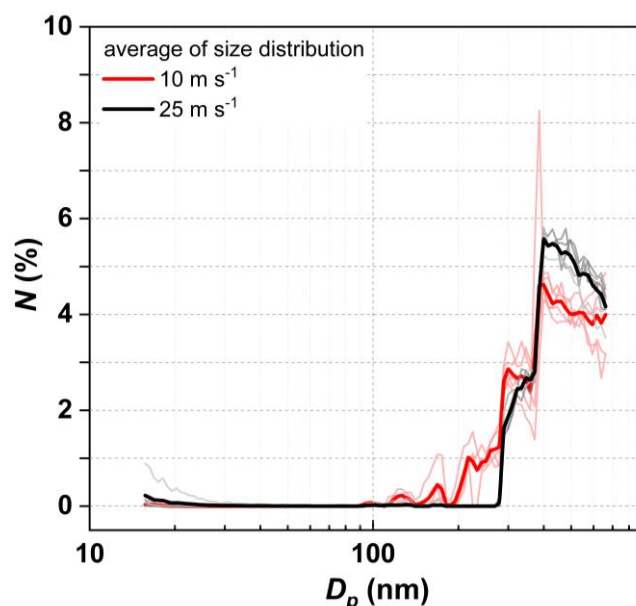

Figure S5. The average size distributions of aerosols generated at different wind speed conditions (red line for 10 m s^{-1} and black line for 25 m s^{-1}). The solid lines with faint color are the size distributions of aerosols obtained at different time after filling the tank (red lines for 10 m s^{-1} and gray lines for 25 m s^{-1}).
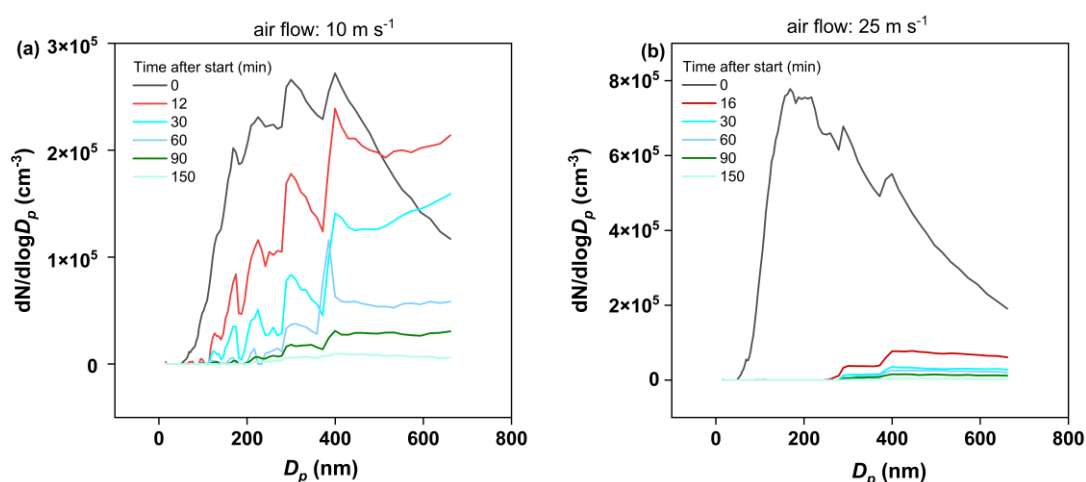

Figure S6. The size distributions of particles in the mixing tank as a function of time after burning under two different wind speed conditions (a) 10 m s^{-1} and (b) 25 m s^{-1}.
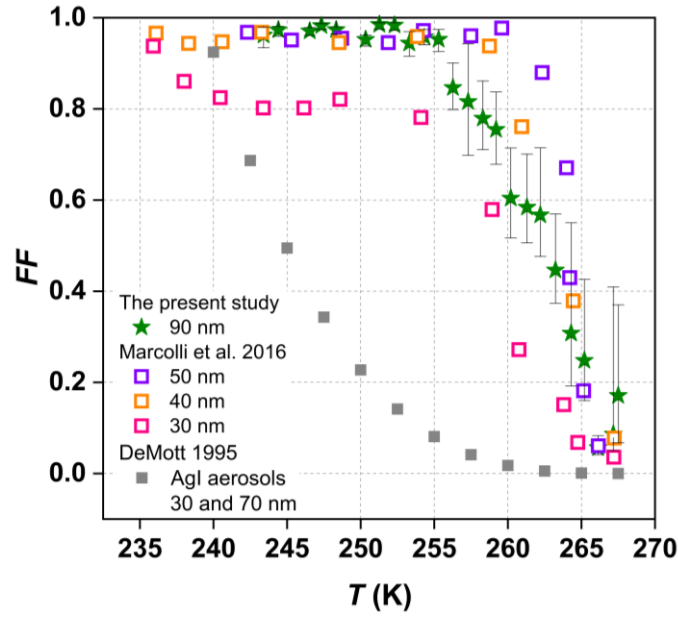
Figure S7. Frozen fraction (FF) as a function of temperature of 90 nm AgI containing flare-generated aerosols compared to AgI particles from other studies [*DeMott*, 1995; *Marcolli et al.*, 2016]. *Marcolli et al.* [2016] generated pure AgI particles (30 nm-50 nm) from the AgI-water suspension; The gray values are calculated based on the ice nucleation parameterization of AgI-containing aerosols (30 nm and 70 nm) developed by *DeMott* [1995], where the aerosols were generated by burning AgI–acetone–ammonium iodide–water solutions in a propane flame.
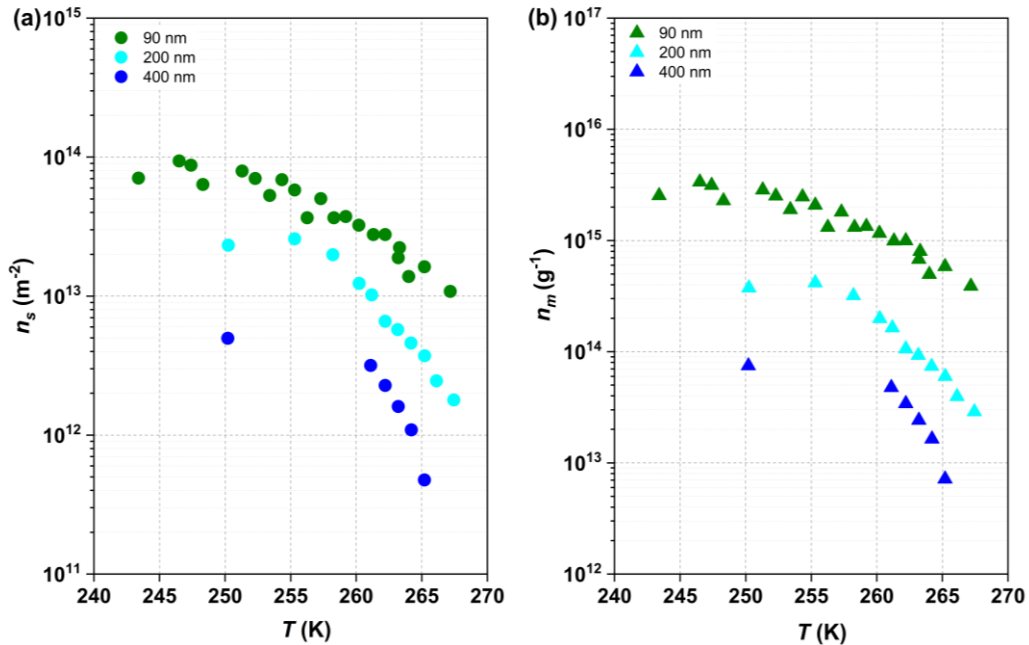

Figure S8. The active site densities per unit particle surface (n_s) and per unit particle mass (n_m) as a function of immersion freezing temperature of AgI-containing aerosol produced by burning the burn-in-place flares, for three different aerosol diameters

(90 nm, 200 nm, 400 nm). n_s and n_m was derived based on Eq. (4) and Eq. (3) assuming spherical particle shape and corresponding geometric surface area.

Table S1. Mode sizes (nm) of the generated aerosols depending on wind speeds (m s^{-1}) and the flare diameter (D_p) from a wind tunnel. Data courtesy of Dr. Aleksei Shilin.

	Wind Speed (m s^{-1})							
D_p (mm)	1	5	10	20	30	40	55	70
7	168	95	84	-	**52**	41	34	29
10	186	112	91	67	59	51	44	33
13	194	113	107	68	67	53	49	38
16	167	125	102	73	64	54	50	43
18	110	112	117	75	63	55	52	45
20	121	127	-	80	68	54	52	51
24	152	130	121	88	72	63	55	**52**

Table S2. The average particle mass measured by CPMA with respect to the particle size.

Particle diameter (nm)	Average measured particle mass (fg)
90	0.48[⊥]
200	7.70
400	33.48

⊥ calculated value based on CPMA measurements of 200 nm and 400 nm particles.

References

DeMott, P. J. (1995), Quantitative descriptions of ice formation mechanisms of silver iodide-type aerosols, *Atmospheric Research*, *38*(1), 63-99.

Earle, M. E., T. Kuhn, A. F. Khalizov, and J. J. Sloan (2010), Volume nucleation rates for homogeneous freezing in supercooled water microdroplets: results from a combined experimental and modelling approach, *Atmos. Chem. Phys.*, *10*(16), 7945-7961.

Ickes, L., A. Welti, C. Hoose, and U. Lohmann (2015), Classical nucleation theory of homogeneous freezing of water: thermodynamic and kinetic parameters, *Physical Chemistry Chemical Physics*, *17*(8), 5514-5537.

Lüönd, F., O. Stetzer, A. Welti, and U. Lohmann (2010), Experimental study on the ice nucleation ability of size-selected kaolinite particles in the immersion mode, *Journal of Geophysical Research: Atmospheres*, *115*(D14).

Marcolli, C., B. Nagare, A. Welti, and U. Lohmann (2016), Ice nucleation efficiency of AgI: review and new insights, *Atmos. Chem. Phys.*, *16*(14), 8915-8937.

Welti, A., F. Lüönd, Z. A. Kanji, O. Stetzer, and U. Lohmann (2012), Time dependence of immersion freezing: an experimental study on size selected kaolinite particles, *Atmos. Chem. Phys.*, *12*(20), 9893-9907.